Journal of Power Sources 195 (2010) 3508–3512

Contents lists available at ScienceDirect

Journal of Power Sources

journal homepage: www.elsevier.com/locate/jpowsour

Short communication

Steady liquid water saturation distribution in hydrophobic gas-diffusion layers with engineered pore paths: An invasion-percolation pore-network analysis

Kyu-Jin Lee[a], Jung Ho Kang[a], Jin Hyun Nam[b,*], Charn-Jung Kim[a]

[a] School of Mechanical and Aerospace Engineering, Seoul National University, Seoul 151-742, Republic of Korea
[b] School of Mechanical and Automotive Engineering, Kookmin University, 861-1 Jeongneung-dong, Seongbuk-gu, Seoul 136-702, Republic of Korea

ARTICLE INFO

Article history:
Received 2 September 2009
Received in revised form 7 October 2009
Accepted 18 November 2009
Available online 23 December 2009

Keywords:
Polymer electrolyte membrane fuel cell
Hydrophobic gas-diffusion layer
Liquid water transport
Saturation distribution
Engineered pore path
Invasion-percolation process

ABSTRACT

The modification of pore structures in gas-diffusion layers (GDLs) has long been studied in the context of efforts to facilitate liquid water transport and to reduce flooding. Such improvements can theoretically improve the performance of polymer electrolyte membrane fuel cells (PEMFCs). Recent experimental studies have demonstrated that engineered pore paths in hydrophobic GDLs, in the form of either large vertical slits or holes, can be advantageous for water management in PEMFCs. In this study, a pore-network model is employed to obtain the steady saturation distribution of liquid water in hydrophobic GDLs with several engineered pore paths. The pore-network results clearly indicate the merits of engineered pore paths in reducing liquid water saturation levels in hydrophobic GDLs. The mechanism by which these engineered pore paths reduce liquid water flooding is discussed in reference to the invasion-percolation process in porous media.

1. Introduction

Polymer electrolyte membrane fuel cells (PEMFCs) are expected to become important power sources in many applications [1,2]. Water management in gas-diffusion layers (GDLs) is currently being researched extensively as part of efforts to improve the power density of PEMFCs. This is because electrode flooding significantly impairs the performance of PEMFCs, especially at high current densities [3,4]. The modification of pore structures in hydrophobic GDLs has been attempted as a means of enhancing the water transport properties of GDLs. The application of a microporous layer (MPL) on the catalyst layer (CL) side of a GDL is a typical example of pore structure modification [5–8]. In addition, bi-modal pore-size distributions or spatially varying pore structures have been studied to enhance the water management properties of GDLs and MPLs [9–13].

Recent experimental studies have demonstrated that engineered pore paths formed in hydrophobic GDLs, such as large vertical slits [14] or holes [15], can enhance the performance of PEMFCs, especially under operating conditions of high current density. The merits of large straight paths in GDLs may be due to an increased permeability for liquid water transport from the viewpoint of continuum two-phase flow theories. Alternatively, the role of such paths may be understood from an invasion-percolation viewpoint [16–18] in the context of liquid water transport in hydrophobic GDLs. Liquid water penetrates more easily into larger pores with lower capillary entry pressures, a feature that can lower the saturation level in GDLs by reducing the random invasion-percolation process. As a result, the effective separation of liquid transport paths and gas-diffusion paths is further facilitated in hydrophobic GDLs, and will lead to improved PEMFC performance.

Continuum two-phase flow models have been used to simulate liquid water transport and to determine saturation distribution in hydrophobic GDLs [19–24]. Continuum models have also been employed to evaluate the capillary effect due to the layer-by-layer variation of pore structures [21,22]. These models cannot, however, easily treat the spatial inhomogeneity that results from the engineered pore paths formed in otherwise homogeneous GDLs. Computational fluid dynamics (CFD) and the lattice Boltzmann method (LBM) provide a fundamental approach to evaluate the capillary transport of liquid water in hydrophobic GDLs with engineered pore paths, but these methods tend to suffer from excessive computational cost. Several pore-network studies have recently been developed to solve the detailed liquid water transport in GDLs with relatively small computational cost [16,18,25–29]. The results have shown that invasion-percolation with capillary dendrite-like penetration, or 'fingering', is prevalent in liquid water transport in hydrophobic GDLs.

In this study, the saturation distribution of liquid water in hydrophobic GDLs with, or without, engineered pore paths is deter-

* Corresponding author. Tel.: +82 2 910 4858; fax: +82 2 910 4839.
E-mail address: akko2@kookmin.ac.kr (J.H. Nam).

0378-7753/$ – see front matter © 2009 Elsevier B.V. All rights reserved.
doi:10.1016/j.jpowsour.2009.11.141

mined based on a steady pore-network model developed by Lee et al. [18]. Three types of engineered pore paths are considered, namely, vertical paths, horizontal paths that reside at the bottom of a GDL and thus contact with a CL or a MPL, and a combination of the two types. The liquid water saturation and the capillary pressure levels in hydrophobic GDLs with different engineered pore paths are compared. Subsequently, the approximate regions of percolated liquid water clusters are visualized. The mechanisms by which these engineered pore paths can reduce the saturation level in hydrophobic GDLs are also investigated.

2. Theory and calculations

Pore-network studies have recently demonstrated that liquid water transport in hydrophobic GDLs is a strongly capillary-driven process, primarily due to the very small flow rate of liquid water in PEMFCs [16,18,25–29]. The capillary number, $Ca = \mu_{inv} q_{inv}/\sigma \cos\theta_c$, is estimated to be only about 10^{-7} to 10^{-8} for PEMFCs operating at 1–2 A cm^{-2}, which leads to negligible viscous effects as compared with capillary effects. According to the phase diagram proposed by Lenormand et al. [30], invasion-percolation with active capillary fingering (the capillary fingering regime) should be a main transport mechanism for liquid water transport in hydrophobic GDLs. In addition, Lenormand et al. [30] showed that continuum two-phase flow models become less valid for the capillary fingering regime with diminishingly small Ca numbers. Recent high-resolution neutron imaging studies [31,32] have also reported liquid water saturation distributions in GDLs that do not generally agree with continuum model predictions.

In this study, the liquid water saturation in hydrophobic GDLs, without and with engineered pore paths, is simulated based on a steady pore-network model recently published by Lee et al. [18]. This model first determines the essential transport paths based on an invasion-percolation procedure that continuously searches for the largest transport paths for liquid water penetration. Then, the steady viscous flow of liquid water through the percolated clusters is solved iteratively while simultaneously updating the transport paths according to the calculated capillary pressure. Finally, the spatial distribution of the liquid water saturation in GDLs is determined based on the calculated capillary pressures in the percolated clusters. In this study, however, only the invasion-percolation calculation is performed to determine the steady distribution of liquid water saturation and capillary pressure in hydrophobic GDLs. In fact, the results of Lee et al. [18] demonstrate that liquid water transport in hydrophobic GDLs almost reaches the pure invasion-percolation limit with $Ca \approx 0$ for a current density range of 1–2 A cm^{-2}. A similar invasion-percolation pore-network model was independently developed by Ceballos and Prat [29].

The pore-network geometry considered in this investigation is shown in Fig. 1(a), where the domain of a GDL is divided into regularly stacked cubic cells. Each of the cubic cells is composed of a box-shaped pore in the centre and six box-shaped constrictions or 'throats' in the faces. Two neighbouring pores are allowed to interact with each other only through these throats. The edge length of the cubic cells, L_{cell}, is set to 25 μm, and three edge lengths of the box-shaped pores are randomly chosen to be between $0.7L_{cell}$ and $0.9L_{cell}$ (17.5–22.5 μm). Similarly, two edge lengths of the box-shaped throats are randomly chosen to be between $0.2L_{cell}$ and $0.7L_{cell}$ (5–17.5 μm). The boundary conditions are also given in Fig. 1(a). Liquid water is assumed to be injected into the pore-network from the bottom plane (inlet) and to be exhausted through the top plane (outlet). To simulate the spatially uniform flux of liquid water from a CL or an MPL, 25% of the pores in the bottom plane are randomly chosen as inlet pores for liquid water injection. Cyclic connectivity is assumed for the side planes in order to extend the calculation domain infinitely in planar directions. For more detailed information on the steady pore-network model, refer to Lee et al. [18].

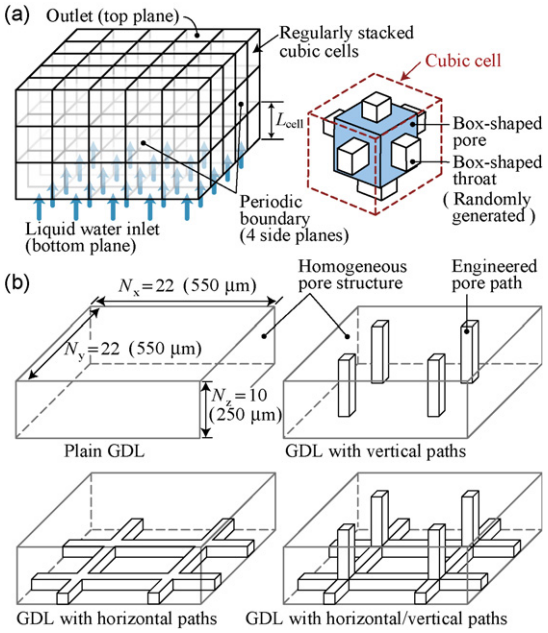

Fig. 1. Steady pore-network model: (a) pore-network geometry; (b) GDLs without and with engineered pore paths.

Fig. 1(b) shows the four types of GDLs without and with the engineered pore paths for preferential liquid water transport considered in this analysis, i.e., a plain GDL, and GDLs with vertical paths, horizontal paths, or both (denoted as horizontal/vertical paths). Note that the vertical paths are similar to the laser perforated holes considered by Gerteisen et al. [15]. The individual vertical paths are assumed to penetrate a GDL straight down from the top plane to the bottom plane. Similarly, the horizontal paths are assumed to have cross-linked shapes and to reside in the bottom plane of a GDL. In order to form engineered paths in a randomly generated pore-network, the edge lengths for the pores and throats in those paths are reassigned to larger values, i.e., $0.95L_{cell}$ (23.75 μm) for selected pores and $0.9L_{cell}$ (22.5 μm) for selected throats. The pore structures outside the engineered pore paths remained homogenous.

The size of the simulated pore-networks is $22 \times 22 \times 10$ in terms of cell numbers, or $550 \times 550 \times 250$ μm in terms of lengths, as shown in Fig. 1(b). Of the 484 total pores in the bottom plane, 121 are randomly selected as the inlet pores for liquid water injection, with an inlet flooding probability, P_f^o, of 25% [18].

3. Results and discussion

Due to the random nature inherent in the pore-network calculations, a total of 100 pore-network realizations are randomly generated and calculated for each of the GDL types as shown in Fig. 1(b). The pore-network results are summarized in Table 1 in terms of an average value and a standard deviation. The average porosity of the simulated pore-networks is estimated to be around 0.63–0.64. The data in Table 1 clearly indicate that the average liquid water saturation can be considerably reduced through the formation of engineered pore paths in hydrophobic GDLs. A maximum reduction of about 30% is expected for the average saturation level when horizontal/vertical paths are formed in

Table 1
Summary of pore-network simulation results.

Parameters	Plain GDL	GDL with vertical paths	GDL with horizontal paths	GDL with horizontal/vertical paths
Porosity	0.634[a] ± SD[b] 0.001	0.635 ± SD 0.001	0.638 ± SD 0.001	0.640 ± SD 0.001
Flooded pore fraction	0.382 ± SD 0.029	0.337 ± SD 0.028	0.321 ± SD 0.031	0.264 ± SD 0.027
Water saturation	0.286 ± SD 0.021	0.255 ± SD 0.021	0.245 ± SD 0.023	0.205 ± SD 0.020
Breakthrough number density	17.0 ± SD 5.7 mm^{-1}	24.0 ± SD 5.2 mm^{-1}	9.6 ± SD 4.9 mm^{-1}	20.9 ± SD 4.4 mm^{-1}
Saturation reduction	100%	88.9%	85.6%	71.7%

[a] Averaged value of 100 pore-network realizations for each GDL type.
[b] SD denotes standard deviation.

hydrophobic GDLs. It appears that the number of breakthrough sites is reduced by about 30% on account of the horizontal paths formed in hydrophobic GDLs. By contrast, the other engineered pore paths seem to increase the number of breakthrough sites from GDLs.

For a more detailed investigation of the effects of engineered pore paths, the spatial distributions of layer-by-layer averaged parameters are plotted in Fig. 2 for the flooded pore fraction, f_p, the liquid water saturation, s_w, and the capillary pressure, p_c. The fraction of flooded pores, f_p, decreases almost linearly from about 0.75 near the inlet to 0.06 near the outlet. It should be noted that f_p near the inlet boundary is much higher than the prescribed inlet flooding probability, P_f^o, of 25%. This is because additional pores near the inlet boundary become flooded during invasion-percolation transport of liquid water in hydrophobic GDLs. When engineered pore paths are formed in GDLs, f_p falls to a lower level and its variation transforms into a concave shape. The vertical paths and horizontal paths appear to reduce f_p by a similar degree, but the combination of the two results in a more pronounced reduction in f_p. A slight increase in f_p is apparent near the inlet boundary for the GDL with horizontal paths, which is due to the presence of large engineered pores in that region.

The distribution of the liquid water saturation, s_w, which is determined by considering the liquid water contents in both the pores and the throats, is presented in Fig. 2(b). Since about 80% of the total void volume is associated with the pores in the present pore-network geometry, it is not surprising that the distribution of s_w is similar to that of f_p. Thus, the lowest saturation level is obtained for GDLs with horizontal/vertical paths.

The distribution of capillary pressure, p_c, is illustrated in Fig. 2(c). Note that p_c is obtained by algebraically averaging the capillary pressures in flooded pores. While the vertical paths and the horizontal paths exhibit relatively similar behaviour for f_p in Fig. 2(a) and for s_w in Fig. 2(c), the p_c values for the two engineered pore paths show quite different trends in Fig. 2(c). The vertical paths generally lower the value of p_c throughout the GDL region, while the horizontal paths cause a reduction in p_c only near the inlet boundary. When horizontal/vertical paths are formed in GDLs, p_c is reduced even further as shown in Fig. 3(c). In addition, p_c is remarkably low near the inlet boundary, most likely due to the presence of large engineered pores in that region.

The approximate distribution of liquid water saturation in the GDLs without and with engineered pore paths is presented in Fig. 3. For a direct comparison of the influence of each engineered pore path, results from an identical pore-network are presented. It should be noted that the data in Fig. 3 ignores the presence of solid structures and therefore only illustrates approximate regions of liquid water. More information regarding the interpretation of Fig. 3 can be found in Lee et al. [18]. The engineered pore paths, represented as dashed circles in Fig. 3, are found to reduce considerably the saturation level, while also leading to a simpler structure of percolated liquid water clusters in the GDLs. This is because the engineered pore paths are preferentially used for liquid water transport, thereby reducing random invasion-percolation with capillary fingering.

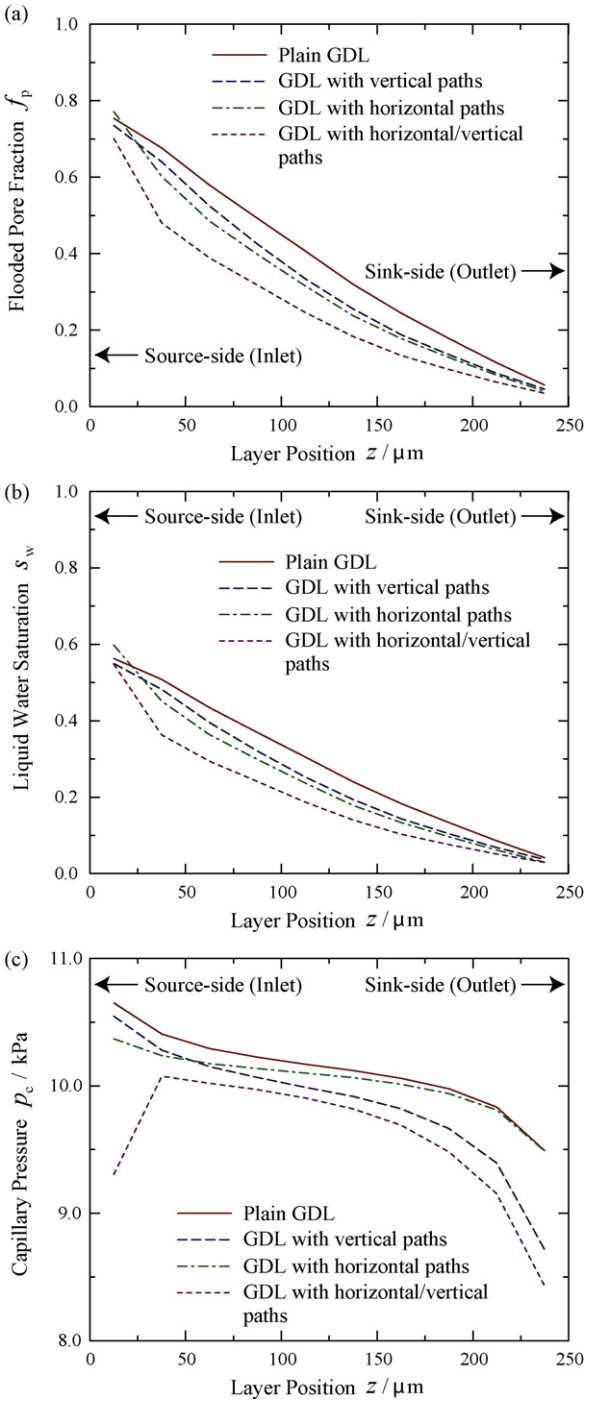

Fig. 2. Spatial distributions of layer-by-layer averaged parameters: (a) flooded pore fraction, f_p; (b) liquid water saturation, s_w; (c) capillary pressures, p_c.

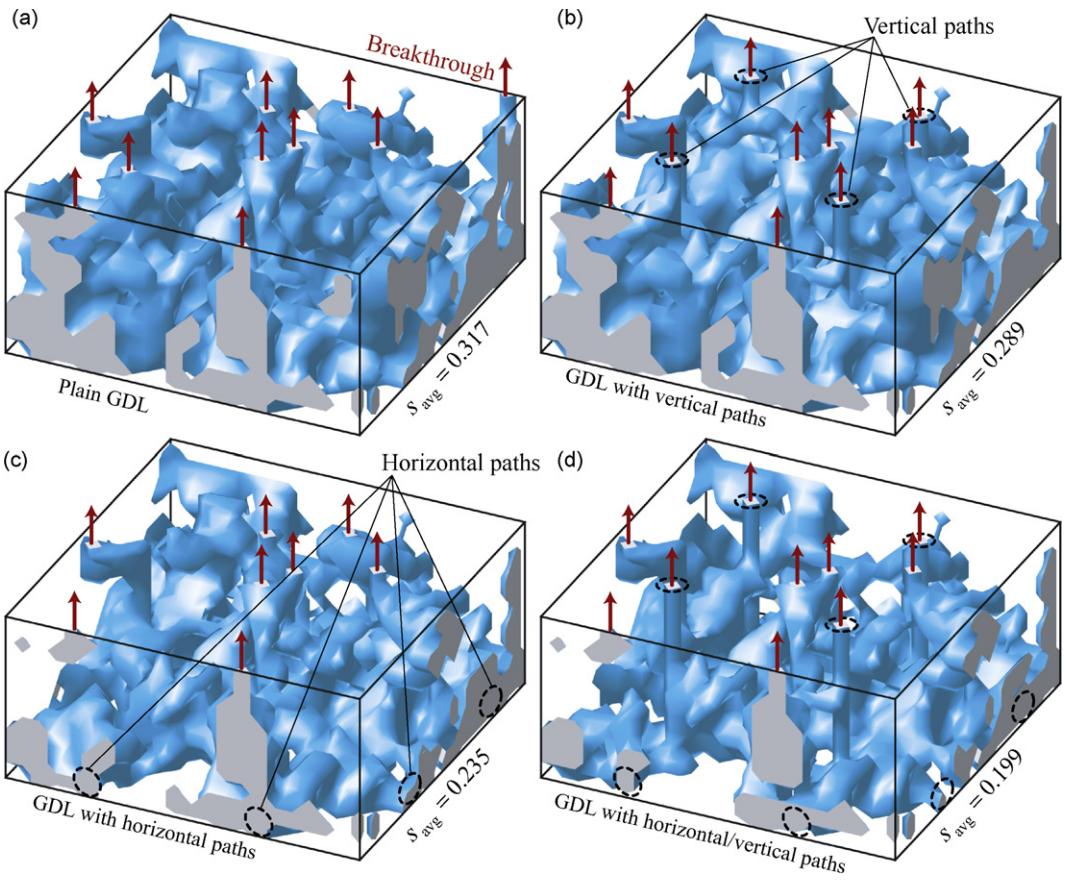

Fig. 3. Approximate distribution of liquid water saturation in an identical pore-network: (a) GDL without engineered pore paths; (b) GDL with vertical paths; (c) GDL with horizontal paths; (d) GDL with horizontal/vertical paths.

The advantage of the vertical paths formed in GDLs can be easily understood from the perspective of invasion-percolation water transport. Liquid water flows primarily through the vertical paths when capillary fingering fronts meet those paths during random invasion-percolation in hydrophobic GDLs. Thus, excessive capillary fingering of liquid water is avoided, and the saturation level is reduced. The advantage of straight vertical paths in hydrophobic GLDs has been demonstrated experimentally by Gerteisen et al. [15]. It should be noted that continuum two-phase flow theories might also explain the advantage of vertical engineered paths to some degree. That is, straight vertical paths provide preferential transport paths in GDLs with less viscous resistance and there by increased permeability values. This, in turn, decreases the capillary pressure level that is required for two-phase flow and this results in reduced liquid water saturation.

The advantage of horizontal engineered paths at the inlet plane of the GDLs shown in Fig. 3(c) cannot be predicted by continuum two-phase flow theories. Pore-network studies by Lee et al. [18] demonstrated that a spatially uniform pressure condition at the inlet boundary results in a much smaller saturation level in GDLs as compared with a spatially uniform flux condition. This is closely related to the findings of invasion-percolation pore-network studies [18,29] show that the saturation level in GDLs is strongly dependent on the number of injection sites at the inlet boundary. From the viewpoint of the invasion-percolation transport, horizontal engineered paths formed near the inlet boundary of GDLs greatly facilitate the merging of liquid water transport paths which, in turn, effectively prevents excessive capillary fingering. In addition, horizontal engineered paths lead to a more uniform pressure at the inlet boundary due to their substantial flow conductance.

4. Conclusions

A steady pore-network calculation based on pure invasion-percolation transport is performed to evaluate the saturation reduction in hydrophobic GDLs, each with a different engineered pore path. The pore-network simulation shows that vertical and horizontal engineered paths can reduce the average saturation levels in hydrophobic GDLs by about 11 and 14%, respectively. The GDLs with combined horizontal/vertical engineered paths are predicted to result in about 30% lower average saturation levels as compared with plain GDLs. The mechanism by which the saturation level is reduced can be explained from the viewpoint of invasion-percolation transport of liquid water in hydrophobic GDLs.

References

[1] A. Dicks, J. Larminie, Fuel Cell Systems Explained, 2nd ed., John Wiley & Sons, New York, 2003.
[2] R. O'Hayre, S.W. Cha, W. Colella, F.B. Prinz, Fuel Cell Fundamentals, John Wiley & Sons, New York, 2005.
[3] H. Li, Y. Tang, Z. Wang, Z. Shi, S. Wu, D. Song, J. Zhang, K. Fatih, J. Zhang, H. Wang, Z. Liu, R. Abouatallah, A. Mazza, J. Power Sources 178 (2008) 103–117.
[4] N. Yousfi-Steiner, Ph. Moçotéguy, D. Candusso, D. Hissel, A. Hernandez, A. Aslanides, J. Power Sources 183 (2008) 260–274.
[5] M.S. Wilson, J.A. Valerio, S. Gottesfeld, Electrochim. Acta 40 (1995) 355–363.
[6] V.A. Paganin, E.A. Ticianelli, E.R. Gonzalez, J. Appl. Electrochem. 26 (1996) 297–304.
[7] Z. Qi, A. Kaufman, J. Power Sources 109 (2002) 38–46.
[8] S. Park, J.W. Lee, B.N. Popov, J. Power Sources 163 (2006) 357–363.
[9] C.S. Kong, D.Y. Kim, H.K. Lee, Y.G. Shul, T.H. Lee, J. Power Sources 108 (2002) 185–191.
[10] X.L. Wang, H.M. Zhang, J.L. Zhang, H.F. Xu, X.B. Zhu, J. Chen, B.L. Yi, J. Power Sources 162 (2006) 474–479.
[11] G.G. Park, Y.J. Sohn, S.D. Yim, T.H. Yang, Y.G. Yoon, W.Y. Lee, K. Eguchi, C.S. Kim, J. Power Sources 163 (2006) 113–118.

[12] H.L. Tang, S.L. Wang, M. Pan, R.Z. Yuan, J. Power Sources 166 (2007) 41–46.
[13] M. Han, J.H. Xu, S.H. Chan, S.P. Jiang, Electrochim. Acta 53 (2008) 5361–5367.
[14] K. Nishida, T. Murakami, S. Tsushima, S. Hirai, Electrochemistry 75 (2007) 149–151.
[15] D. Gerteisen, T. Heilmann, C. Ziegler, J. Power Sources 177 (2008) 348–354.
[16] K.J. Lee, J.H. Nam, C.J. Kim, Electrochim. Acta 54 (2009) 1166–1176.
[17] J.H. Nam, K.J. Lee, G.S. Hwang, C.J. Kim, M. Kaviany, Int. J. Heat Mass Transfer 52 (2009) 2779–2791.
[18] K.J. Lee, J.H. Nam, C.J. Kim, J. Power Sources 195 (2010) 130–141.
[19] Z.H. Wang, C.Y. Wang, K.S. Chen, J. Power Sources 94 (2001) 40–50.
[20] L.X. You, H.T. Liu, Int. J. Heat Mass Transfer 45 (2002) 2277–2287.
[21] J.H. Nam, M. Kaviany, Int. J. Heat Mass Transfer 46 (2003) 4595–4611.
[22] U. Pasaogullari, C.Y. Wang, Electrochim. Acta 49 (2004) 4359–4369.
[23] A.Z. Weber, J. Newman, J. Electrochem. Soc. 152 (2005) A677–A688.
[24] G.Y. Lin, T.V. Nguyen, J. Electrochem. Soc. 153 (2006) A372–A382.
[25] P.K. Sinha, C.Y. Wang, Electrochim. Acta 52 (2007) 7936–7945.
[26] P.K. Sinha, C.Y. Wang, Chem. Eng. Sci. 63 (2008) 1081–1091.
[27] O. Chapuis, M. Prat, M. Quintard, E. Chane-Kane, O. Guillot, N. Mayer, J. Power Sources 178 (2008) 258–268.
[28] M. Rebai, M. Prat, J. Power Sources 192 (2009) 534–543.
[29] L. Ceballos, M. Prat, J. Power Sources 195 (2010) 825–828.
[30] R. Lenormand, E. Touboul, C. Zarcone, J. Fluid Mech. 189 (1988) 165–187.
[31] M.A. Hickner, N.P. Siegel, K.S. Chen, D.S. Hussey, D.L. Jacobson, M. Arif, J. Electrochem. Soc. 155 (2008) B427–B434.
[32] C. Hartnig, I. Manke, R. Kuhn, N. Kardjilov, J. Banhart, W. Lehnert, Appl. Phys. Lett. 92 (2008) 134106.